Journal of Food Measurement and Characterization (2021) 15:3408–3418
https://doi.org/10.1007/s11694-021-00920-y

ORIGINAL PAPER

Inhibitory kinetics and mechanism of oleanolic acid on α-glucosidase

Zhike Xie[1] · Ming He[1] · Yuhan Zhai[1] · Feifei Xin[1] · Shuyan Yu[1] · Shaoxuan Yu[1] · Haifang Xiao[1] · Yuanda Song[1]

Received: 19 December 2020 / Accepted: 3 April 2021 / Published online: 21 April 2021
© The Author(s), under exclusive licence to Springer Science+Business Media, LLC, part of Springer Nature 2021

Abstract

Inhibition of α-glucosidase is considered as an effective approach to treat type 2 diabetes. Therefore, it is of great significance to study the inhibition of this enzyme. In the present study, the inhibitory activity of oleanolic acid (OA) on α-glucosidase and their interaction mechanism were investigated. The inhibition kinetic analysis showed that OA reversibly inhibited α-glucosidase activity in a mixed-type manner with an IC_{50} value of 3.04 ± 0.05 μM, and the inhibition followed a multi-phase kinetic process with a first-order reaction. The change of enthalpy and entropy indicated that the binding of OA to glucosidase was mainly driven by hydrophobic interaction and hydrogen bonding, and the binding distance was estimated at 3.51 nm. Synchronous fluorescence, circular dichroism (CD) and Fourier transform infrared spectra (FT-IR) showed that the binding of OA to α-glucosidase induced rearrangement and conformational changes of the enzymes. The molecular docking illustrated that OA entered the active center of α-glucosidase and interacted with the amino acid residues Asp-352 and ultimately inhibiting the enzyme activity.

Keywords α-Glucosidase · Oleanolic acid · Inhibitory kinetics · Inhibition mechanism

Introduction

Diabetes mellitus (DM) is a serious worldwide problem and urgently needs further consideration. According to the World Health Organization, diabetes will be the 7th leading cause of death globally by 2030 [1]. DM is mainly divided into type 1 diabetes, type 2 diabetes, gestational diabetes and uncommon types of diabetes relying on their pathogenesis. The typical characteristic of type 2 diabetes is hyperglycemia, which will induce many complications including uremia, renal failure, neuropathy, and cardiovascular disease [2]. This form of diabetes is associated with an excessive intake of foods rich in fast-digesting carbohydrates, such as starch and its derivatives [3]. Starches are broken down into sugars in the body by digestive enzymes such as α-glucosidase. Rapid release of glucose in the gastrointestinal tract leads to elevated blood sugar levels, which in turn increases the risk of diabetes [4]. Therefore, inhibition of α-glucosidase hydrolysis to release glucose is an effective method to reduce postprandial hyperglycemia [5].

In clinical practices, a limited number of known α-glucosidase inhibitors, including miglitol, acarbose and 1-doxycycline (DNJ), are widely used in the treatment of type 2 diabetes. However, the extensive use of these inhibitors is limited by their complex manufacturing process, high cost and side effects including abdomen pain, diarrhea, flatulence and skin problems [6]. Therefore, there is an urgent need to discover better plant-based foods or supplements as alternatives to α-glucosidase inhibitors because of their low cost and relative safety. Natural products have been always the most important and productive sources of compounds in drug development. Several potent α-glucosidase inhibitors have been found in natural products, such as kaempferol, tannic acid, procyanidin dimer and luteolin [7–10]. Oleanolic acid (OA), a pentacyclic triterpene, is found in many fruits and vegetables, such as olive leaves (*Olea Europaea*), mistletoe sprouts (*Viscum album*), grape (*Vitis Vinifera*) and clove (*Syzylium aromaticum*). Preliminary study found that OA possessed a potent antioxidant activity and exhibited great protective effect on oxidative stress induced by tert-butyl hydrogen peroxide in liver cells [11]. Besides, OA improved obesity-related hyperlipidemia and protected against endothelial dysfunction in hypertensive patients [12,

✉ Haifang Xiao
xiaohaifang@sdut.edu.cn

[1] School of Agricultural Engineering and Food Science, Shandong University of Technology, Zibo 255049, Shandong, China

13], and inhibited 11β-hydroxysteroid dehydrogenase type 1 (11betβ-HSD1) in the liver and peripheral tissues [14]. Although OA has an inhibitory effect on Brewer's Yeast α-glucosidase activity, the inhibitory mechanism of OA on α-glucosidase is still unclear.

In this study, UV-vis absorption, fluorescence, CD, FT-IR, kinetic analysis and molecular docking methods were used to study the inhibitory effect of OA on α-glucosidase in vitro and its mechanism. The binding characteristics of OA and α-glucosidase were characterized, and the microenvironment and secondary structure changes of α-glucosidase induced by OA were measured. This study provides new insights into the mechanisms by which OA inhibits α-glucosidase activity, which will help to develop more effective functional foods and supplements for the treatment of type 2 diabetes.

Materials and methods

Materials

α-glucosidase (from *Saccharomyces cerevisiae*, EC 3.2.1.20, Molecular Weight: 63,000) and OA (purity ≥ 98 %) were purchased from Shanghai Yuanye Biotechnology Co. (Shanghai, China). α-glucosidase was prepared in sodium phosphate buffer (0.1 M, pH 6.8), while OA was made in dimethyl sulfoxide (DMSO). The final amounts of DMSO throughout experiments were below 1% (v/v), which did not have negative effect on α-glucosidase. Acarbose and p-nitrophenyl-α-D-glucopyranoside (pNPG) were purchased from Aladdin Chemical Co. (Shanghai, China). All other chemicals and solvents were analytical quality, and fresh ultrapure water was used in all the experiments.

α-Glucosidase inhibitory activity assay

The inhibitory activity of OA against α-glucosidase was evaluated using the previous method with slight alterations [7, 15]. In brief, α-glucosidase with a fixed final concentration (2 μM) and a series of different concentrations of OA were mixed in sodium phosphate buffers (0.1 M, pH 6.8) and incubated for 2 h at 37 °C. pNPG (final concentration 400 μM) used as a substrate was added to the OA-enzyme complex solution to initiate the reaction. The absorbance of the mixtures was monitored at 405 nm every 10 s by a Microplate reader. Acarbose was used as a positive control. IC_{50} was defined as the concentration required for the inhibitor to reduce 50 % enzymatic activity. The enzymatic activity assay without inhibitor was defined as 100%. Relative enzymatic activity (%) = (slope of reaction kinetics equation obtained by the reaction with inhibitor)/ (slope of reaction kinetics equation obtained by the reaction without inhibitor) × 100 [16].

Kinetics involved in the inhibition of α-glucosidase

The inhibition was evaluated according to the Lineweaver–Burk equation. The mixed inhibition was expressed by Eq. [7]:

$$\frac{1}{\nu} = \frac{K_m}{V_{max}}\left(1 + \frac{[I]}{K_i}\right)\frac{1}{[S]} + \frac{1}{V_{max}}\left(1 + \frac{[I]}{K_{is}}\right) \quad (1)$$

Secondary plots were constructed from

$$\text{Slope} = \frac{K_m}{V_{max}} + \frac{K_m[I]}{V_{max}K_i} \quad (2)$$

and

$$Y\text{-intercept} = \frac{1}{V_{max}^{app}} = \frac{1}{V_{max}} + \frac{1}{K_{is}V_{max}}[I] \quad (3)$$

where K_i and K_{is} represent the equilibrium constant for inhibitor binding with free enzyme and the enzyme-substrate complex, respectively. And K_m is the Michaelis-Menten constant. ν is the enzyme reaction rate with or without OA. I and S represent the OA (0, 2, 4, 6, and 8 μM) and pNPG (0.2, 0.4, 0.6, 0.8 and 1.0 μM), respectively.

Fluorescence spectra analysis

A 2.5 ml of α-glucosidase solution (3 μM) was titrated serially with an increasing amount of OA solution (to obtain various concentrations from 0 to 33.0 μM). The excitation wavelength was set at 280 nm and the emission spectra were collected from 300 to 450 nm, and both the excitation and emission slits were set at 3.0 nm. Fluorescence spectra were conducted at three different temperatures (298, 304, and 310 K) on a spectrofluorometer equipped with a 1.0 cm path-length quartz cell and thermostat bath. These mixtures were allowed to stand for 5 min and then their fluorescence spectra were determined.

The synchronous fluorescence spectra were determined by setting the excitation and emission wavelength interval (Δλ) at 15 and 60 nm, with the slit widths of both were set at 3.0 nm.

All the fluorescence intensities were corrected because of the absorption of both excited and emitted light to eliminate any re-absorption [17].

$$F_{corr} = F_{obs}e^{(A_1+A_2)/2} \quad (4)$$

where F_{corr} and F_{obs} denote the corrected and observed fluorescence intensities. A_1 and A_2 represent the absorbance of OA at excitation and emission wavelengths, respectively.

CD measurement

CD spectra were scanned on a CD spectrometer (Bio-Logic, Claix, France) over the range of 190–250 nm. The concentration of α-glucosidase was fixed on 3.0 μM while varying the OA concentration from 0 to 16.0 μM ([OA]/[α-glucosidase] = 0:1, 1:1, 4:1 and 8:1). The CD spectra were an average of three scans under constant nitrogen flush and buffer signal was subtracted. The contents of different secondary structures of α-glucosidase were analyzed by using the Dichroweb online analysis system (http://dichroweb.cryst.bbk.ac.uk/html/home.shtml). Firstly, the ASCII file containing the CD data was imported into the online analysis system. The initial wavelength was set as 250 nm, the final wavelength was set as 190 nm, and the wavelength step was set as 1 nm. Select SELCON 3 and Set 1 as the analysis program and reference set, respectively.

FT-IR spectra analysis

FT-IR spectra of free α-glucosidase (6 μM) and its OA complex were determined according to the previous methods with some modifications [17]. The FT-IR spectrometer at wavenumbers between 1600 and 1700 cm^{-1} in pH 6.8 sodium phosphate buffer with the resolution of 4 cm^{-1} and 60 scans and all spectra were taken via the ATR. The final concentration of OA was 10.0 μM. The corresponding absorbance values related to free OA and buffer solutions were recorded and subtracted at the same instrumental parameters. FT-IR spectra analysis was used to obtain resolution on secondary structures of α-glucosidase by curve-fitted results of amide I band.

Docking simulation

The possible interaction between glucosidase and OA was further analyzed by the docking program (AutoDock 4.2, Scripps, USA). Download the crystal structure of α-glucosidase (PDB ID:3A4A) from the protein database (http://www.rcsb.org/pdb) and check for any errors. In this process, all water molecules were removed, polar hydrogen atoms and Kollman charges were added to the protein, and then the Gasteiger charges were calculated. The 3D structure of OA was formed in Chem3D Ultra 8.0. In the docking process, Lamarckian Genetic Algorithm (LGA) was selected to conduct ligand conformation search. The grid box size was set as (80 Å × 80 Å × 90 Å) and a grid spacing of 0.375 Å. The conformation with the lowest energy and more docking number at the same time was selected as the best binding mode for further analysis.

Statistical analysis

The results were expressed as the mean values ± standard deviations, and all determinations were performed in triplicate. One-way analysis of variance (ANOVA) was implemented by using Origin 8.0 followed by multiple tests in order to determine the significant difference at $p < 0.05$.

Results and discussion

Inhibitory effect of OA on α-glucosidase in vitro

As shown in Fig. 1A, OA exhibited expected inhibition on α-glucosidase in a dose-dependent manner, the enzymatic activity declined rapidly till almost totally inhibited with the increase of OA concentration from 0 to 14 μM. In addition, the values of IC_{50} for OA and acarbose were calculated to be (3.04 ± 0.05) μM and (25.83 ± 1.23) μM, respectively. These results indicated that OA was a powerful α-glucosidase inhibitor *in vitro*. The IC_{50} value of OA on α-glucosidase was lower than the previous report (12.8 ± 0.00) [18]. This might be due to the manufacturer of the OA, and the measurement methods and conditions. Previous study found that ursolic acid with a similar structure to OA exhibited inhibition of α-glucosidase with IC_{50} values of 5.04 μM [19]. Compared to ursolic acid, OA inhibited α-glucosidase more effectively. This may be probably due to the fact that OA has two methyl groups C-20, whereas ursolic acid has two methyl groups C-19 and C-20 in the ortho position of the E ring [20]. The reversibility of OA-mediated inhibition was shown in Fig. 1B. All the lines were linear and passed through the origin, and the slope decreased with the increase of OA concentration. These results confirmed the reversibility of OA in α-glucosidase inhibition [21].

Kinetic mode of inhibition of OA on α-glucosidase

Lineweaver–Burk plots were employed to investigate the inhibition type of OA to α-glucosidase. The double reciprocal plots were obtained as shown in Fig. 2A. All the lines fitted linearly and intersected in second quadrant. Furthermore, the apparent K_m and V_{max} changed simultaneously, and the value of V_{max} decreased as K_m increased. The results indicated that OA induced mixed-type inhibition [22]. The secondary plots (inset of Fig. 2A) showed a good linear relationship, suggesting that OA had a single inhibition site or a single class of inhibition sites on α-glucosidase. Based on Eqs. (2) and (3), the K_i and K_{is} values were calculated to be (5.81 ± 0.45) μM and (21.76 ± 1.06) μM, respectively. Obviously, the value of K_{is} was greater than K_i, meaning that the

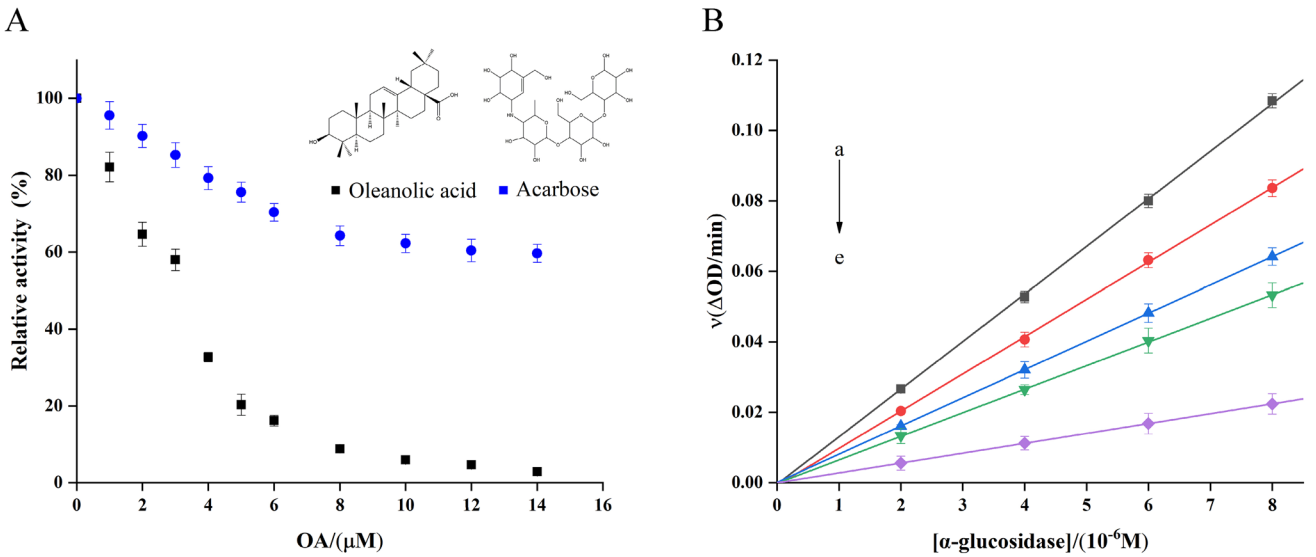

Fig. 1 **A** Inhibitory effects OA on α-glucosidase (pH 6.8, T = 310 K). **B** Plots of ν versus [α-glucosidase]. c(pNPG) = 400 μM, c(OA) = 0, 1, 2, 4, 6, and 8 μM for curves a → e, respectively

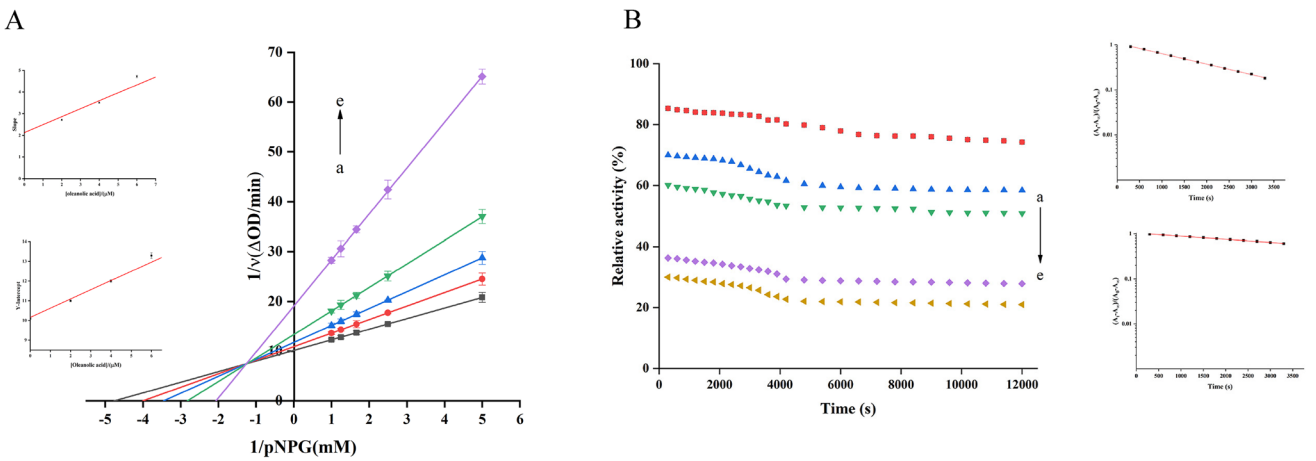

Fig. 2 **A** Lineweaver–Burk plots. c[α-glucosidase] = 2 μM, and c(OA) = 0, 2, 4, 6, and 8 μM for curves a → e, respectively. The secondary plots of slope (the upper left) and Y-intercept (the lower left) vs. [OA] were in the inset. **B** Kinetic time courses for change of absorption value of α-glucosidase in the presence of OA at 2, 4, 6, 8, and 10 μM for curves a → e, respectively. Semilogarithmic plots c(OA) = 10 μM (upper right), c(OA) = 2 μM (lower right)

affinity between inhibitor and enzyme was stronger than that of enzyme-substrate complex [23].

Inactivation kinetics and rate constants

In order to determine the inactivation kinetics and the rate constant, the inhibitory effect of OA at different concentrations on α-glucosidase was studied (Fig. 2B). The catalytic activity of α-glucosidase declined detectably in the first 4000 s whereafter remained stable. Subsequent analysis of semilogarithmic plots showed that the inactivation process followed first-order kinetics. The partial inactivation process was monophasic without the formation of intermediates. The inactivation rate constants (k) were calculated from the right plots of Fig. 2B and summarized in Table 1. The transition free energy change (ΔΔG°) can be calculated by $\Delta\Delta G^\circ = -RT\ln k$, and the changes of ΔΔG° resulted in the inactivation of α-glucosidase [24].

Fluorescence quenching of α-glucosidase by OA

The binding of OA and α-glucosidase was studied by fluorescence spectrometry. α-glucosidase has endogenous fluorescent chromophores, such as tryptophan, tyrosine and

Table 1 Inactivation rate constants for α-glucosidase in the presence of OA

OA (μM)	Inactivation rate constants ($\times 10^{-4}$ s^{-1}), k[a]	Transition free-energy change[b] (kJ mol^{-1} s^{-1})
2.00	2.32	21.57
4.00	1.87	22.12
6.00	1.29	23.08
8.00	0.70	24.66
10.00	0.68	24.74

[a]k is the first-order rate constant

[b]Transition free-energy change pers is $\Delta\Delta G^{\circ} = -RT \ln k$, where k is a time constant of the inactivation reaction

phenylalanine, all of which were aromatic amino acids [25]. The tryptophan and tyrosine residues as the main source of intrinsic fluorescence properties of α-glucosidase can be used to determine inhibitor combined with enzyme binding constant, binding sites and mechanism [15]. Fluorescence quenching can be caused by many factors, including molecular hind course, excited state reaction and interaction with small molecules. All quenching mechanisms can be divided into two categories: dynamic quenching and static quenching [26]. Thus, the intrinsic fluorescence of α-glucosidase in the absence and presence of OA was studied at three different temperatures (298, 304 and 310 K). As shown in Fig. 3A, when excited at 280 nm, the fluorescence emission peak of free α-glucosidase appeared near 340 nm and

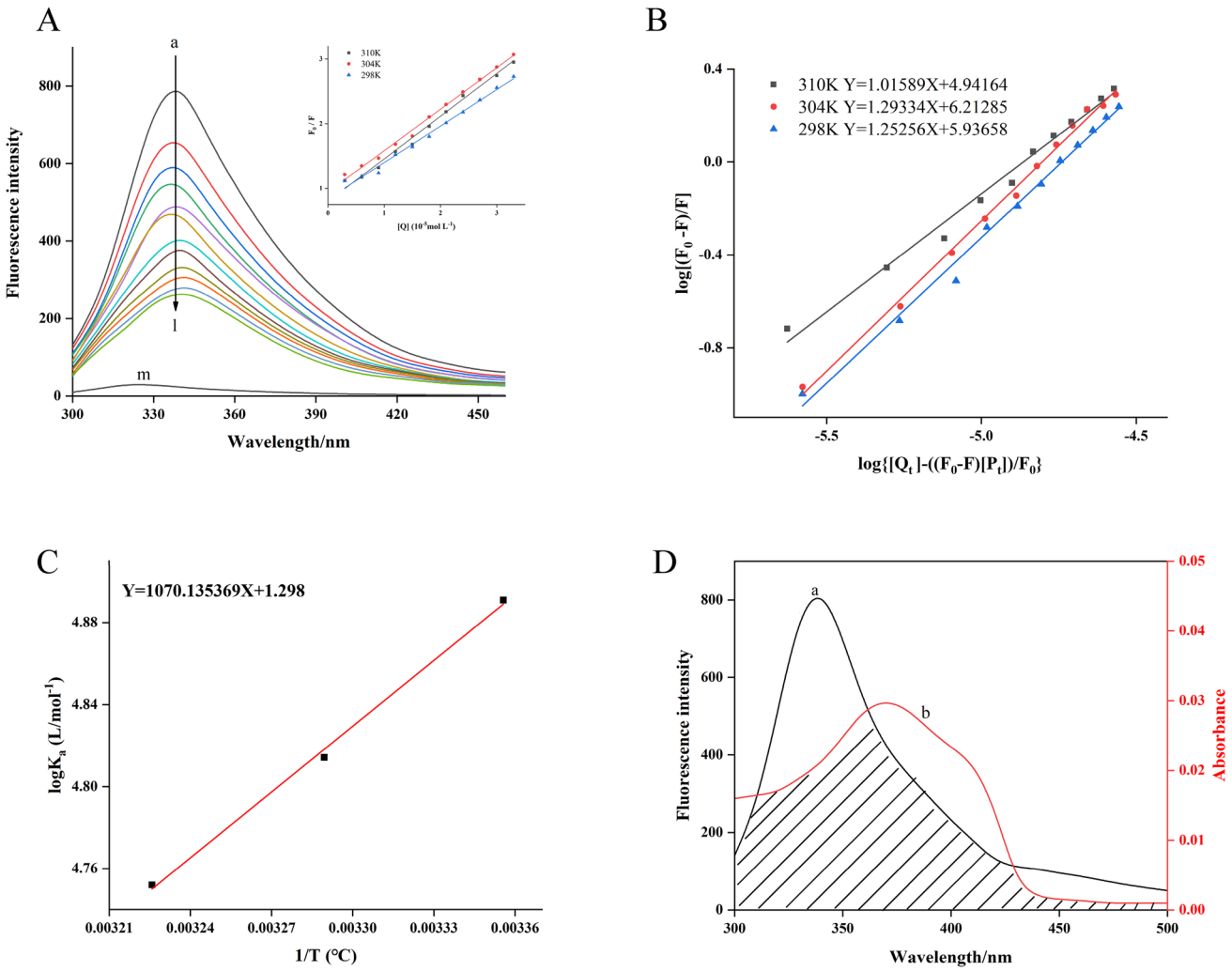

Fig. 3 **A** Fluorescence spectra of α-glucosidase in the absence and presence of OA with various concentrations (pH 6.8, l_{ex}= 280 nm). c(α-glucosidase) = 3.0 μM, and c(OA) = 0, 3.0, 6.0, 9.0, 12.0, 15.0, 18.0, 21.0, 24.0, 27.0, 30.0 and 33.0 μM for curves a → l, respectively. Curve m shows the emission spectrum of OA at the concentration of 3.0 μM. The inset shows Stern-Volmer plots for the fluorescence quenching of α-glucosidase by OA at three different temperatures. **B** Plots of log $(F_0 - F)/F$ versus log([Q_t] − [P_t] $(F_0 - F)/F$) for the interaction of OA and α-glucosidase. **C** Plot of log Ka versus $1/T$ for the interaction of OA and α-glucosidase. **D** Spectral overlaps of the fluorescence spectrum of α-glucosidase (a) with the absorption spectrum of OA (b). c(α-glucosidase) = c(OA) = 3.0 μM

the OA itself did not show fluorescence. The fluorescence intensity of α-glucosidase decreased dramatically with the increase of OA concentration, while the shift in the position of the emission peak was not detected. The phenomenon would be direct evidence for the interaction between OA and α-glucosidase.

To further investigate the quenching mechanism and determine the quenching constants (K_{sv}), Stern–Volmer equation was employed as followed [27]:

$$\frac{F_0}{F} = 1 + K_{SV}[Q] = 1 + K_q \tau_0 [Q] \quad (5)$$

where F_0 and F are the fluorescence intensities in the absence and presence of quencher, respectively. [Q] is the concentration of quencher. K_{sv} is the Stern-Volmer quenching constant, which could be calculated by linear regression of a plot of F_0/F against [Q]. K_q is the biomolecule quenching rate constant ($K_q = K_{SV}/\tau_0$). τ_0 is the average lifetime of the fluorophore in the absence of the quencher (the value is 10^{-8} s) [28].

The values of K_{SV} from the plot of F_0/F versus [Q] (inset of Fig. 3A) at three different temperatures (298, 304 and 310 K) were listed in Table 2. All the three lines showed good linearity, suggesting that the quenching mechanism might be either a dynamic or static procedure. The values of K_{SV} decreased with the increase of temperature, and the K_q values at three temperatures (298, 304, and 310 K) were 6.59×10^{12}, 6.40×10^{12}, and 5.64×10^{12} L mol^{-1} s^{-1}, respectively, which were two orders of magnitude greater than the maximum diffusion collision quenching constant (2.0×10^{-10} L mol^{-1} s^{-1}). These results indicated that the fluorescence quenching of α-glucosidase was a static quenching, resulting from the formation of enzyme-OA complex [29].

Binding constant and number of binding sites

To determine the binding constant (K_a) and number of binding sites (n), the double-logarithm regression plot was built according to the following relationship [30] :

$$\log\frac{F_0 - F}{F} = n\log K_a - n\log\frac{1}{[Q_t] - \frac{(F_0 - F)[P_t]}{F_0}} \quad (6)$$

where F_0 and F are the same with Eq. (5); [P_t] and [Q_t] mean the total concentrations of the α-glucosidase and OA, respectively. The values of K_a and n were calculated from the slope and intercept of Fig. 3B, and the results were summarized in Table 2. The values of n at 298, 304 and 310 K were approximately equal to 1, indicating that there was only a single binding site on α-glucosidase for OA [31], which supported the result of the Lineweaver–Burk plot analysis that OA bound in a single class of inhibition site on α-glucosidase.

The value of K_a was inversely correlated with temperature, suggesting that the stability of the OA-α-glucosidase complex decreased at a higher temperature. Those results also further proved that the fluorescence quenching was a static quenching process [32].

Thermodynamic analysis and binding forces

In order to further characterize the intermolecular forces between α-glucosidase and OA, the thermodynamic parameters were estimated. The interaction between a small ligand and a biomolecule comes into being a supramolecular complex usually by the four main forces: hydrophobic interaction,electrostatic force, hydrogen bond and van der Waals force. Thus, the thermodynamic parameters including enthalpy ($\Delta H°$),entropy change ($\Delta S°$) and free energy change ($\Delta G°$) were calculated by the Van't Hoff equation as followed [33]:

$$\log K_a = -\frac{\triangle H°}{2.303RT} + \frac{\triangle S°}{2.303R} \quad (7)$$

$$\triangle G° = \triangle H° - \triangle TS° \quad (8)$$

where K_a is the binding constant at the corresponding temperature (T), T is the absolute temperature (298, 304 and 310 K). The values of $\Delta S°$ and $\Delta G°$ were calculated from the slope and intercept of the linear plot of log Ka versus $1/T$ (Fig. 3C). R is the gas constant (8.314 J mol^{-1} K^{-1}). The negative values of $\Delta G°$ meant that the binding was a spontaneous process. The values of $\Delta H°$ and $\Delta S°$ were calculated to be -20.49 ± 0.30 kJ mol^{-1} and 24.85 ± 0.2 J mol^{-1} K^{-1} respectively (Table 2). According to the theory of Ross and Subramanian [34], $\Delta H° < 0$ and $\Delta S° > 0$ indicated that hydrophobic forces and hydrogen bonding played a predominant role in the interaction between OA and α-glucosidase.

Binding distance

According to the overlapping spectra of the fluorescence spectrum of α- glucosidase and ultraviolet absorption spectrum of OA, and according to Förster's non-radiative energy transfer theory, the binding position distance between the small molecules of binding protein and tryptophan residues in protein sequence can be determined [35]. The distance r between the donor and acceptor could be calculated by the following equations:

$$E = \frac{F_0 - F}{F_0} = \frac{R_0^6}{R_0^6 + r^6} \quad (9)$$

$$R_0^6 = 8.79\times10^{-25}\kappa^2 N^{-4}\phi J \quad (10)$$

$$J = \frac{\sum F(\lambda)\varepsilon(\lambda)\lambda^4\Delta\lambda}{\sum F(\lambda)\Delta\lambda} \quad (11)$$

where F_0 and F are the same as in Eq. (5). R_0 denotes the critical distance when the transfer efficiency is 50%. r is the distance between OA and α-glucosidase. κ^2 is the orientation factor of dipole. N is the refractive index of the medium. ϕ is the fluorescence quantum yield of α-glucosidase (ϕ = 0.118) [36], and J represents the overlap integral between the donor fluorescence emission spectrum and the acceptor absorption spectrum (Fig. 3D). In this study, $\kappa^2 = 2/3$, $N = 1.336$. The values of the parameters were $J = 1.18 \times 10^{-14}$ cm^3 L mol^{-1}, $R_0 = 2.52$ nm, $E = 0.12$, and $r = 3.51$ nm. The value of r was less than 8 nm and $0.5R_0 < r < 1.5R_0$, suggesting that the non-radiative energy transfer from α-glucosidase to OA might occurred [37]. Furthermore, $r > R_0$ further supported that this fluorescence quenching was static between OA and α-glucosidase [38].

Change in conformation of α-glucosidase induced by OA

Synchronous fluorescence spectroscopy is an effective method to determine the microenvironmental changes of fluorophore (tyrosine and tryptophan residues) by measuring the possible spectral shifts in the maximum emission wavelength [39]. As shown in Fig. 4A–B, the fluorescence intensities of both tyrosine and tryptophan residues decreased regularly when the concentration of OA increased, but their maximum emission wavelength did not shift obviously, indicating that the polarity and hydrophobicity around tyrosine and tryptophan residues were not significantly affected by OA [40].

For confirming the conformational changes of α-glucosidase induced by OA, the CD spectra of α-glucosidase were measured with various amounts of OA. It was found that the spectra of α-glucosidase presented two negative bands at 206 and 218 nm (Fig. 4C), which were characteristic of α-helix of protein [41]. The signal strength of the two negative bands decreased regularly without any significant changes in the peak position and shape upon the addition of OA, indicating a reduction in helicity of α-glucosidase due to the binding of OA. The contents of different secondary structures of α-glucosidase were calculated by the online SELCON3 program. With the increase in molar ratios of OA to α-glucosidase (from 0:1 to 1:1, 4:1, 8:1), and the calculated contents of α-helix and random coil decreased from16.54–15.61%, 15.40%, 5.01% and from 30.91–29.46%, 28.10%, 24.87%, respectively. While the percentages of β-sheet and β-turn contents increased from 29.70–32.0%, 33.40%, 35.65% and from 22.85–22.93%, 23.10%, 24.47%, respectively. These results suggested that the binding of OA to α-glucosidase might lead to the unfolding of part of the constitutive polypeptide, thus affecting the conformation of α-glucosidase and inhibiting the enzyme activity. In addition, due to the peak position and peak shape of the enzyme did not change significantly, it indicated that the basic structure of the enzyme remained unchanged after the combination with OA.

Further evidence for the structural changes of α-glucosidase was obtained from FT-IR measurements. FT-IR spectrum is usually used to study the secondary structure of protein, which is due to the existence of many amide bands, which represent various vibrations of peptide moiety. The amide groups of peptides and proteins show a characteristic vibrational mode (amide mode), which is very sensitive to the conformational change of protein secondary structure and largely constrained to group frequency interpretations [42]. Three amide bands including amide I, II and III could be clarified according to the absorption peaks of proteins in different ranges of wavenumbers, and amide I, mainly originated from the C=O stretching vibration, was widely used to study the protein secondary structures [43]. In addition, the secondary structure of α-glucosidase was changed by calculating the percentage of β-antiparallel, β-turn, α-helix, random coil and β-sheet. The results were shown in Fig. 4D; Table 3. When the final concentration of OA was reached to 1×10^{-5} mol L^{-1} in the α-glucosidase solution, the percentages of α-helix and random coil were decreased from 29.95–21.19% and 28.89–15.66%, respectively. However, the β-antiparallel, β-turn and β-sheet contents were increased to 8.50%, 23.42 and 31.23%, respectively. These results showed that the interaction between OA and the C=O group in the protein subunits changed the secondary structure of α-glucosidase [44]. These results were consistent with that obtained from CD analysis.

Computational docking of OA on α-glucosidase

Molecular docking as a complementary application has recently been widely used to further demonstrate drug-protein interactions [41]. The α-glucosidase structure model was built based on a high sequence homology (PDB ID: 3A4A; gi number 411229) [45]. The cluster with the lowest energy (– 6.16 kcal mol^{-1}) and the second most frequent trajectory (32 out of 100, the red bar in Fig. 5A) was selected from 100 docking operations as the best cluster for combining direction analysis. The predicted binding energy was a little bit higher than ΔG° (– 6.66 kcal mol^{-1}) acquired from the thermodynamic analysis at 298 K, which might be due to the lack of desolvation energy as the molecular docking was carried out under simulation of the vacuum condition.

As shown in Fig. 5B, OA obviously easily entered the active site of α-glucosidase and was surrounded by the

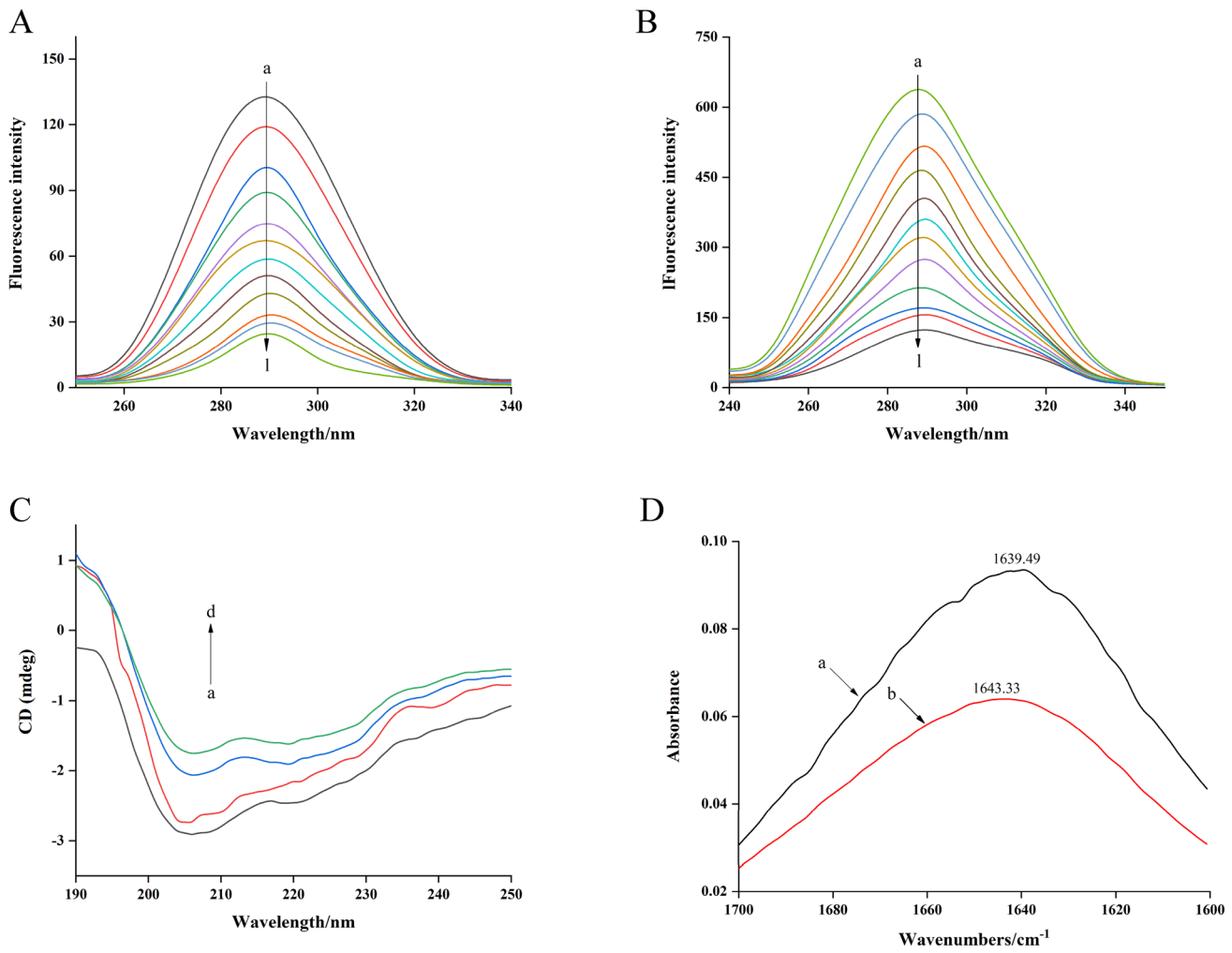

Fig. 4 Synchronous fluorescence spectra of α-glucosidase in the absence and presence of OA. **A** Δλ = 15 nm, **B** Δλ = 60 nm. (pH 6.8, T = 298 K). c(α-glucosidase) = 3.0 μM. c(OA) = 0, 3.0, 6.0, 9.0, 12.0, 15.0, 18.0, 21.0, 24.0, 27.0, 30.0 and 33.0 μM for curves a → l, respectively. **C** The CD spectra of α-glucosidase in the presence of increasing amounts of OA. c(α-glucosidase) = 3 μM, the molar ratios of OA to α-glucosidase were 0:1 (a), 1:1 (b), 4:1 (c) and 8:1 (d), respectively. **D** The FT-IR spectra of free α-glucosidase (a) and OA-α-glucosidase complex (b) at room temperature in the region of 1700–1600 cm^{-1}

Table 2 Quenching constants K_{SV}, binding constants K_a, and relative thermodynamic parameters for the interaction of OA with α-glucosidase at different temperatures

T(K)	K_{sv} ($\times 10^4$ L mol^{-1})	R^a	K_a ($\times 10^4$ L mol^{-1})	*n*	R^b	$\Delta H°$ (kJ mol^{-1})	$\Delta G°$ (kJ mol^{-1})	$\Delta S°$ (J mol^{-1} K^{-1})
298	6.59 ± 0.02	0.9890	7.78 ± 0.03	1.01 ± 0.03	0.9880	− 20.49 ± 0.30	− 27.8953 ± 0.20	24.85 ± 0.20
304	6.40 ± 0.01	0.9953	6.52 ± 0.02	1.29 ± 0.03	0.9958		− 28.0444 ± 0.20	
310	5.64 ± 0.02	0.9905	5.65 ± 0.03	1.25 ± 0.03	0.9726		− 28.1935 ± 0.20	

[a]*R* is the correlation coefficient for the K_{SV} values. [b]R is the correlation coefficient for the K_a values

catalytic amino acid residues Gln-353, Asp-307, Glu-411, Arg-315, Asp-352, Tyr-158, Arg-213 and His-280. OA seemed to be effectively bound to the active site of α-glucosidase and thereby inhibited the catalytic activity. Moreover, a hydrogen bond formed (yellow dashed line) with Asp-352 (1.94Å). These results indicated that the binding of OA to α-glucosidase was mainly driven by hydrogen bonding, which was confirmed by the above thermodynamic analysis results. Therefore, molecular simulation studies provided some useful information for OA induced inhibition to predict binding sites in the pockets of α-glucosidase activity sites.

Table 3 Influence of OA on the secondary structures of α-glucosidase

Concentrations of OA (μM)	β-Antiparallel (%)	β-Turn (%)	α-Helix (%)	Random coil (%)	β-Sheet (%)
0	3.05	12.15	29.95	28.89	22.96
10	8.50	23.42	21.19	15.66	31.23

Conclusions

This study showed that OA was an effective α-glucosidase inhibitor. OA reversibly inhibited α-glucosidase with the IC_{50} was (3.04 ± 0.05) μM in a mixed-type inhibition through a monophasic process. The fluorescence quenching assay suggested that OA could interact with the α-glucosidase and effectively quench its intrinsic fluorescence in a static quenching mechanism coupled with the formation of OA-α-glucosidase complex. The values of *n* at different temperatures were approximately equal to 1, which indicated that there was a single inhibition site on α-glucosidase for OA. The calculated thermodynamic parameters ΔH° and ΔS° were -20.49 ± 0.30 kJ mol^{-1} and 24.85 ± 0.20 J mol^{-1} K^{-1}, respectively, indicating that the binding of OA to

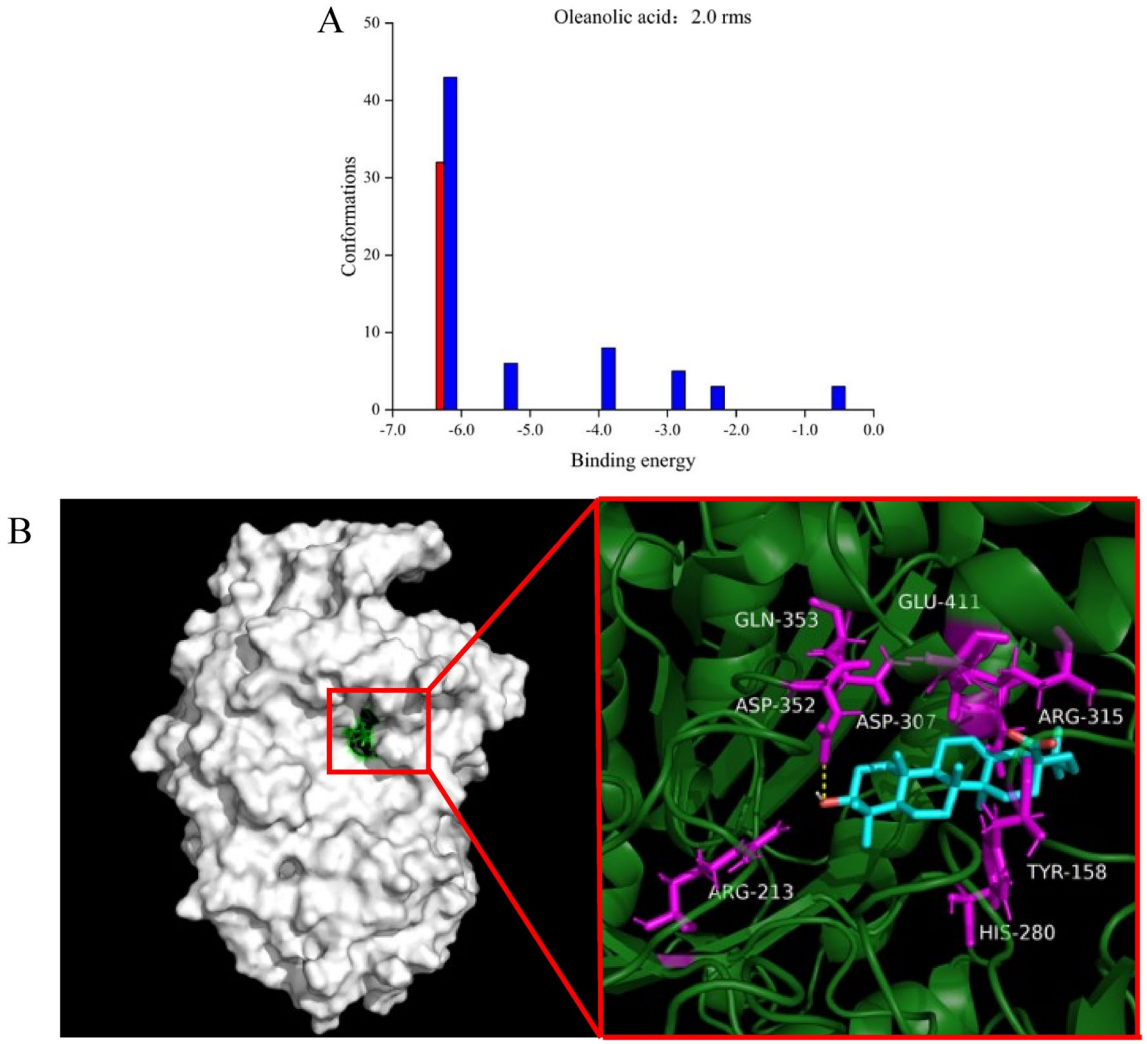

Fig. 5 **A** Cluster analyses of the AutoDock docking runs of OA with α-glucosidase. **B** Predicted binding mode of OA docked with α-glucosidase. The green areas represent the catalytic activity site of α-glucosidase. The blue stick structure was used to represent the OA while the purple stick denotes the residues of α-glucosidase. The short solid yellow line stands for hydrogen bonds

α-glucosidase was dominated mainly by the hydrophobic forces and hydrogen bonding. The results of synchronous fluorescence, CD and FT-IR spectra indicated that OA could interact with α-glucosidase and induced rearrangement and secondary structural changes of the α-glucosidase. Moreover, the results of molecular docking further validated that OA could bind to the catalytic active site of α-glucosidase, hindering the entrance of substrate to inhibit the catalytic activity of α-glucosidase. Those results indicated that OA may be a promising α-glucosidase inhibitor and can be used in further animal studies or clinical trials.

Acknowledgements This work was supported by Shandong Provincial Natural Science Foundation, China (No. ZR2014CQ002), SDUT and Zibo City Integration Development Project (2017ZBXC004). Therefore, we are grateful for the funding and support of this research.

Declarations

Conflict of interest The authors declare that they have no conflict of interest.

References

1. S. Ghosh, P. More, A. Derle, A.B. Patil, P. Markad, A. Asok, N. Kumbhar, M.L. Shaikh, B. Ramanamurthy, V.S. Shinde, D.D. Dhavale, B.A. Chopade, Diosgenin from Dioscorea bulbifera: novel hit for treatment of type ii diabetes mellitus with inhibitory activity against α-amylase and α-glucosidase. PLoS ONE. **9**(9), 106039 (2014)
2. S.W. Leong, F. Abas, K.W. Lam, K. Yusoff, *In vitro* and *in silico* evaluations of diarylpentanoid series as α-glucosidase inhibitor. Bioorg Med Chem Lett. **28**(3), 302–309 (2018)
3. A. Kirakosyan, E. Gutierrez, B. Ramos Solano, E.M. Seymour, S.F. Bolling, The inhibitory potential of Montmorency tart cherry on key enzymes relevant to type 2 diabetes and cardiovascular disease. Food Chem. **252**, 142–146 (2018)
4. M.R. Rekha, C.P. Sharma, Oral delivery of therapeutic protein/peptide for diabetes—Future perspectives. Int J Pharmaceut. **440**(1), 48–62 (2013)
5. Y. Wang, Z. Yang, X. Wei, Sugar compositions, α-glucosidase inhibitory and amylase inhibitory activities of polysaccharides from leaves and flowers of *Camellia sinensis* obtained by different extraction methods. Int J Bio Macromol. **47**(4), 534–539 (2010)
6. P. Gupta, M. Bala, S. Gupta, A. Dua, R. Dabur, E. Injeti, A. Mittal, Efficacy and risk profile of anti-diabetic therapies: conventional vs traditional drugs—a mechanistic revisit to understand their mode of action. Pharmacol Res. **113**, 636–674 (2016)
7. X. Peng, G. Zhang, Y. Liao, D. Gong, Inhibitory kinetics and mechanism of kaempferol on α-glucosidase. Food Chem. **190**, 207–215 (2016)
8. H. Tang, F. Ma, D. Zhao, Z. Xue, Exploring the effect of salvianolic acid C on α-glucosidase: inhibition kinetics, interaction mechanism and molecular modelling methods. Process Biochem. **78**, 178–188 (2019)
9. T. Dai, J. Chen, D.J. McClements, T. Li, C. Liu, Investigation the interaction between procyanidin dimer and alpha-glucosidase: spectroscopic analyses and molecular docking simulation. Int J Biol Macromol. **130**, 315–322 (2019)
10. J. Yan, G. Zhang, J. Pan, Y. Wang, alpha-Glucosidase inhibition by luteolin: kinetics, interaction and molecular docking. Int J Biol Macromol. **64**, 213–223 (2014)
11. X. Wang, X. Ye, R. Liu, H.-L. Chen, H. Bai, X. Liang, X.-D. Zhang, Z. Wang, W. Li, C.-X. Hai, Antioxidant activities of oleanolic acid in vitro: possible role of Nrf2 and MAP kinases. Chem-Biol Interact **184**(3), 328–337 (2010)
12. R. Rodriguez-Rodriguez, M. Herrera, M. Alvarez de Sotomayor, V. Ruiz-Gutierrez, Effects of pomace olive oil-enriched diets on endothelial function of small mesenteric arteries from spontaneously hypertensive rats. Brit J Nutr. **102**, 1435–1444 (2009)
13. K. Yunoki, G. Sasaki, Y. Tokuji, M. Kinoshita, A. Naito, K. Aida, M. Ohnishi, Effect of Dietary Wine Pomace Extract and Oleanolic Acid on Plasma Lipids in Rats Fed High-Fat Diet and Its DNA Microarray Analysis. J. Agric. Food Chem. **56**(24), 12052–12058 (2008)
14. A. Blum, A.D. Favia, E. Maser, 11β-Hydroxysteroid dehydrogenase type 1 inhibitors with oleanan and ursan scaffolds. Mol. Cell. Endocrinol. **301**(1), 132–136 (2009)
15. L. Zeng, H. Ding, X. Hu, G. Zhang, D. Gong, Galangin inhibits α-glucosidase activity and formation of non-enzymatic glycation products. Food Chem. **271**, 70–79 (2019)
16. J. Xie, H. Dong, Y. Yu, S. Cao, Inhibitory effect of synthetic aromatic heterocycle thiosemicarbazone derivatives on mushroom tyrosinase: insights from fluorescence, (1)H NMR titration and molecular docking studies. Food Chem. **190**, 709–716 (2016)
17. L. Han, C. Fang, R. Zhu, Q. Peng, D. Li, M. Wang, Inhibitory effect of phloretin on alpha-glucosidase: kinetics, interaction mechanism and molecular docking. Int J Biol Macromol. **95**, 520–527 (2017)
18. M.I. Choudhary, I. Batool, S.N. Khan, N. Sultana, S.A. Shah, A. Ur-Rahman, Microbial transformation of oleanolic acid by Fusarium lini and alpha-glucosidase inhibitory activity of its transformed products. Nat Prod Res. **22**(6), 489–494 (2008)
19. P.P. Wu, K. Zhang, Y.J. Lu, P. He, S.Q. Zhao, *In vitro* and *in vivo* evaluation of the antidiabetic activity of ursolic acid derivatives. Eur. J. Med. Chem. **80**, 502–508 (2014)
20. Z. Wang, C. Hsu, C. Huang, M. Yin, Anti-glycative effects of oleanolic acid and ursolic acid in kidney of diabetic mice. Eur. J. Pharmacol. **628**(1), 255–260 (2010)
21. D. Xu, Q. Wang, W. Zhang, B. Hu, L. Zhou, X. Zeng, Y. Sun, Inhibitory activities of caffeoylquinic acid derivatives from Ilex kudingcha C.J. Tseng on α-glucosidase from *Saccharomyces cerevisiae*. J. Agric. Food Chem. **63**(14), 3694–3703 (2015)
22. Z. Xiong, W. Liu, L. Zhou, L. Zou, J. Chen, Mushroom *(Agaricus bisporus*) polyphenoloxidase inhibited by apigenin: multi-spectroscopic analyses and computational docking simulation. Food Chem. **203**, 430–439 (2016)
23. J.-P. Zhang, Q.-X. Chen, K.-K. Song, J.-J. Xie, Inhibitory effects of salicylic acid family compounds on the diphenolase activity of mushroom tyrosinase. Food Chem. **95**(4), 579–584 (2006)
24. Q.-X. Jin, S.-J. Yin, W. Wang, Z.-J. Wang, J.-M. Yang, G.-Y. Qian, Y.-X. Si, Y.-D. Park, The effect of Zn2 + on Euphausia superba arginine kinase: unfolding and aggregation studies. Process Biochem. **49**(5), 821–829 (2014)
25. H. Xiao, B. Liu, H. Mo, G. Liang, Comparative evaluation of tannic acid inhibiting α-glucosidase and trypsin. Food Res. Int. **76**(Pt 3), 605–610 (2015)
26. G. Zhang, L. Wang, J. Pan, Probing the binding of the flavonoid diosmetin to human serum albumin by multispectroscopic techniques. J. Agric. Food Chem. **60**(10), 2721–2729 (2012)
27. W.M. Chai, M.K. Wei, R. Wang, R.G. Deng, Z.R. Zou, Y.Y. Peng, Avocado proanthocyanidins as a source of tyrosinase inhibitors: structure characterization, inhibitory activity, and mechanism. J. Agric. Food Chem. **63**(33), 7381–7387 (2015)

28. Y. Yuan, L. Yang, S. Liu, J. Yang, H. Zhang, J. Yan, X. Hu, Enzyme-catalyzed Michael addition for the synthesis of warfarin and its determination via fluorescence quenching of l-tryptophan. Spectrochim Acta A Mol Biomol Spectrosc. **176**, 183–188 (2017)
29. Y. Cui, G. Liang, Y.H. Hu, Y. Shi, Y.X. Cai, H.J. Gao, Q.X. Chen, Q. Wang, Alpha-substituted derivatives of cinnamaldehyde as tyrosinase inhibitors: inhibitory mechanism and molecular analysis. J. Agric. Food Chem. **63**(2), 716–722 (2015)
30. M. Fan, G. Zhang, J. Pan, D. Gong, An inhibition mechanism of dihydromyricetin on tyrosinase and the joint effects of vitamins B6, D3 or E. Food Funct. **8**(7), 2601–2610 (2017)
31. S. Prasanth, D. Rithesh Raj, T.V. Vineeshkumar, R.K. Thomas, C. Sudarsanakumar, Exploring the interaction of l-cysteine capped CuS nanoparticles with bovine serum albumin (BSA): a spectroscopic study. RSC Adv. **6**(63), 58288–58295 (2016)
32. M. Hosseini-Koupaei, B. Shareghi, A.A. Saboury, F. Davar, Molecular investigation on the interaction of spermine with proteinase K by multispectroscopic techniques and molecular simulation studies. Int. J. Biol. Macromol. **94**(Pt A), 406–414 (2017)
33. J. Zhang, Q. Yan, J. Liu, X. Lu, Y. Zhu, J. Wang, S. Wang, Study of the interaction between 5-sulfosalicylic acid and bovine serum albumin by fluorescence spectroscopy. Journal of Lumin. **134**, 747–753 (2013)
34. P.D. Ross, S. Subramanian, Thermodynamics of protein association reactions: forces contributing to stability. Biochemistry. **20**, 3096–3102 (1981)
35. S. Bi, L. Yan, Y. Wang, B. Pang, T. Wang, Spectroscopic study on the interaction of eugenol with salmon sperm DNA in vitro. J Lumin. **132**(9), 2355–2360 (2012)
36. L.L. Zhang, L. Han, S.Y. Yang, X.M. Meng, W.F. Ma, M. Wang, The mechanism of interactions between flavan-3-ols against a-glucosidase and their in vivo antihyperglycemic effects. Bioorg Chem. **85**, 364–372 (2019)
37. Y. Wang, G. Zhang, J. Yan, D. Gong, Inhibitory effect of morin on tyrosinase: insights from spectroscopic and molecular docking studies. Food Chem. **163**, 226–233 (2014)
38. B. Hemmateenejad, M. Shamsipur, F. Samari, T. Khayamian, M. Ebrahimi, Z. Rezaei, Combined fluorescence spectroscopy and molecular modeling studies on the interaction between harmalol and human serum albumin. J. Pharm. Biomed. Anal. **67–68**, 201–208 (2012)
39. S. Roy, R.K. Nandi, S. Ganai, K.C. Majumdar, T.K. Das, Binding interaction of phosphorus heterocycles with bovine serum albumin: a biochemical study. J Pharm Anal. **7**(1), 19–26 (2017)
40. M. Maciazek-Jurczyk, A. Sulkowska, J. Rownicka-Zubik, Alteration of methotrexate binding to human serum albumin induced by oxidative stress. Spectroscopic comparative study. Spectrochim Acta A Mol Biomol Spectrosc. **152**, 537–550 (2016)
41. L. Zeng, G. Zhang, S. Lin, D. Gong, Inhibitory Mechanism of Apigenin on α-Glucosidase and Synergy Analysis of Flavonoids. J. Agric. Food Chem. **64**(37), 6939–6949 (2016)
42. Z. Ganim, A. Tokmakoff, Spectral signatures of heterogeneous protein ensembles revealed by MD Simulations of 2DIR spectra. Biophys J. **91**(7), 2636–2646 (2006)
43. W.K. Surewicz, H.H. Mantsch, D. Chapman, Determination of protein secondary structure by Fourier transform infrared spectroscopy. A critical assessment. Biochemistry-US. **32**(2), 389–394 (1993)
44. P.N. Naik, S.A. Chimatadar, S.T. Nandibewoor, Interaction between a potent corticosteroid drug—dexamethasone with bovine serum albumin and human serum albumin: a fluorescence quenching and fourier transformation infrared spectroscopy study. J. Photochem. Photobiol. B **100**(3), 147–159 (2010)
45. Y. Lee, S. Kim, J.Y. Kim, M. Arooj, S. Kim, S. Hwang, B.-W. Kim, K.H. Park, K.W. Lee, Binding mode analyses and pharmacophore model development for stilbene derivatives as a novel and competitive class of α-glucosidase inhibitors. PLoS ONE. **9**(1), e85827 (2014)

Publisher's note Springer Nature remains neutral with regard to jurisdictional claims in published maps and institutional affiliations.